PIER C

(Received 16 February 2025, Accepted 21 March 2025, Scheduled 22 April 2025)

Theoretical Analysis of Detection of Flying Vehicles Based on the Passive Radiometric Detection of Microwave-Millimeter-Terahertz Wavelength Electromagnetic Emissions from Exhaust Plasma Gases

Thomas N. Chatziathanasiou and Nikolaos Uzunoglu*

Microwave Laboratory, Department of Electrical and Computer Engineering, National Technical University of Athens, Greece

ABSTRACT: The feasibility of using passive radiometric detection of chaotic electromagnetic signals emanating from low density plasma plumes of the jet exhaust gases to detect low radar cross section aircrafts is analyzed for the frequency band 3.10^8–3.10^{12} Hz. The aircraft exhaust plume gas formation is modelled with a number of discrete different dimensions ellipsoids, with each having different electron densities and temperatures. Electromagnetic radiation analysis of emitting signals is computed applying fluctuation-dissipation theorem and geometric considerations. The detection range of characteristic military jet aircraft is computed numerically for the whole frequency band, from UHF to 3 THz. It is shown that high range detection can be achieved at upper microwave frequencies.

1. INTRODUCTION

Stealth technologies pose a challenging problem in early detection of attacking threat aircrafts. During the last decades, several anti-stealth technologies have been proposed such as: (a) use of multi-static radars, (b) use of infrared (IR) detection of thermal radiation emitted from the aircraft exhaust gases and engine outputs, (c) use of low frequency radars (VHF).

Presently, the most widely used anti-stealth technique is the detection of infrared radiation with various alternative receiver types. The drawback of this method could be the absorption of IR radiation from atmospheric phenomena.

In this article, the possibility of using the low edge of electromagnetic spectrum is presented. In principle, the method considered is the same as the IR radiation method. However, the penetration ability into exhaust plume formations at lower frequency electromagnetic waves compared to IR waves necessitates different analysis methods presented here.

2. MODELING OF EXHAUST PLUME OF JET AIRCRAFT

It is well known that exhaust plumes from jet aircraft engines have plasma properties due to the ionization of gases at high temperatures because of the combustion mechanisms. The content of plume gases of aircraft exhausts has been studied by measurements [1, 2].

2.1. Characteristics of Exhaust Plume

The combustion of fossil fuels in a jet aircraft engine produces mainly carbon dioxide (CO_2) (about 6%), water vapor (H_2O) (about 2.5%), nitrogen (N_2) (about 75%), oxygen (O_2) (about 16%), sulfur dioxide (SO_2), and other products of smaller percentages, such as nitrogen oxides (NO_x), unburned hydrocarbons (HC), carbon monoxide (CO), soot (C_{soot}), and sulfur oxides (SO_x). Also, during their combustion in the jet engine, the formation of positive and negative ions is noted [1, 2].

Because of exhaust gases exiting the aircraft engine nozzle into the atmosphere at high velocities (i.e., 750 m/s), having high temperature, gas condensation, high electron density, they have high conductivity [3]. After exhaust gases are extracted from the engine, exhaust plume is formed. The exhaust plume is initialized in time as soon as it leaves the engine nozzle, and because of its flight, it is diluted, creating ionized formations. At the same time, its temperature, electron density, and conductivity are reduced gradually. As a result, a black body type electromagnetic thermal radiation is emitted to the environment from the plume [4].

The exhaust plasma formation in the backward direction of flying aircraft can be approximated in the form of an ellipsoidal shape formation gradually decreasing in density volume, as shown in Fig. 1. Taking the exhaust nozzle as being symmetric, the ellipsoid in most cases can be assumed to be a prolate spheroid that is an ellipsoid with two equal minor axes smaller than the elongated axis opposite to the flight direction. In this study, the plasma volume is approximated as a set of individual coaxial ellipsoids with different plasma characteristics, as shown in Fig. 2. The selection of the number of el-

* Corresponding author: Nikolaos Uzunoglu (nikolaos.uzunoglu@gmail.com).

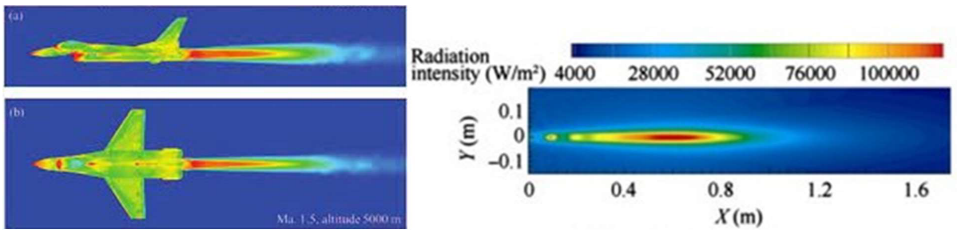

FIGURE 1. Aircraft exhaust plumes.

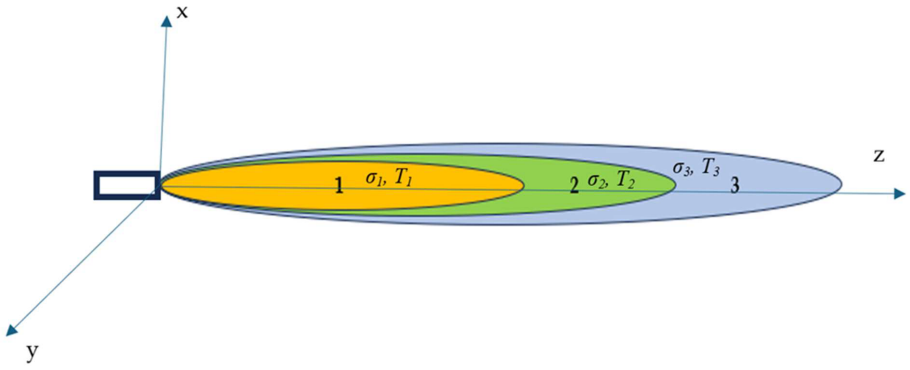

FIGURE 2. Aircraft exhaust plume model using overlapping coaxial ellipsoids. Each region is characterized by its conductivity [Eq. (4)] and temperature measured in Kelvin units.

lipsoids is based on the spatial resolution plasma properties of the plume formation published in the literature which are depicted in present article. Thus, the plasma of each ellipsoid has different characteristics, such as temperature, electron density, electron-ion collision frequencies, and of course the attenuation of electromagnetic waves [3].

Examining the published electron density and temperature distributions, coaxial ellipsoid shape distributions are estimated. In Fig. 2, the adopted model is presented. The coaxial ellipsoids are assumed to have a common "nose point" end, and each region shown in Fig. 2 with indexes $i = 1, 2, ...$ has a specific temperature and electron density.

The electromagnetic properties of a plasma region with electron density Ne (m^{-3}) and collision frequency $\nu\,(\mathrm{Hz}) = {}^{1}\!/_{\tau}$, with τ being the average lifetime of electrons in plasma, are described by a complex relative dielectric constant $\dot{\varepsilon}_r$ in terms of the real numbers ε_r' and ε_r'', as [5]:

$$\dot{\varepsilon}_r = \varepsilon_r^{'} - j\varepsilon_r^{''}, \quad j = \sqrt{-1} \tag{1}$$

$$\varepsilon_r^{'} = 1 - \frac{(\omega_p\tau)^2}{1+(\omega\tau)^2} \tag{2}$$

$\omega_p^2 = \frac{N_e e^2}{m_e \varepsilon_o}$, with ω_p being the plasma frequency, τ = the average electron lifetime because of the electron-ion collisions, $e = 1,62 \times 10^{-19}$ Cb, $m_e = 9,2 \times 10^{-31}$ kg, $\varepsilon_o = 10^{-9}/36\pi$ free space dielectric constant and

$$\varepsilon_r^{''} = \frac{(\omega_p\tau)\,\frac{\omega_p}{\omega}}{1+(\omega\tau)^2} \tag{3}$$

The electrical conductivity of the medium is

$$\sigma = \omega\varepsilon_o\varepsilon_r^{''} \tag{4}$$

and the complex propagation constant of a plane wave inside the plasma is:

$$\dot{k} = \frac{\omega}{c}\sqrt{\varepsilon_r' - j\varepsilon_r''} = k_r - jk_i \tag{5}$$

where $c = 3 \times 10^8$ (m/s) is the free space electromagnetic wave speed while $k_r,\ k_i$ are real numbers.

Introducing Eqs. (2), (3) into (5), since $\omega\tau \gg 1$, the propagation constant when $\omega > \omega_p \gg {}^{1}\!/_{\tau}$ is found to be:

$$k_r \cong \frac{\omega}{c}\sqrt{1 - \frac{(\omega_p\tau)^2}{1+(\omega\tau)^2}} \tag{6}$$

$$k_i \cong \frac{1}{2c}\frac{\omega_p^2\tau}{(\omega\tau)^2 + 1 - (\omega_p\tau)^2} \tag{7}$$

Then in case of a plane wave propagating in a plasma medium, the propagation factor is:

$$e^{-j\dot{k}s} = e^{-k_i s}e^{-jk_r s} \tag{8}$$

where s is the wave travelling axis.

To compute the chaotic radiation emitted by the plume structure shown in Fig. 2, in the first place, the emission from a single ellipsoid shown in Fig. 3 will be examined.

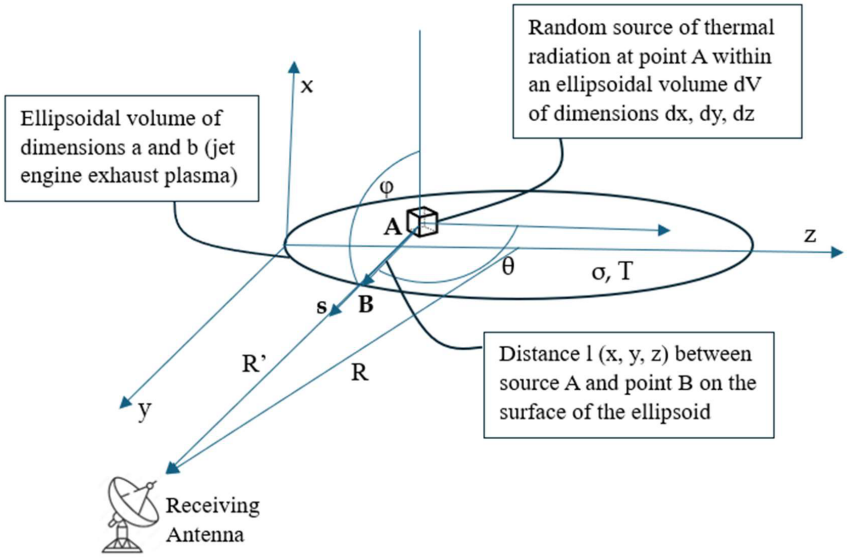

FIGURE 3. An ellipsoid model to compute the received chaotic radiation at a distant antenna.

2.2. Ellipsoid Volume and Electromagnetic Radiation Calculation

Considering an arbitrary elementary volume ΔV (voxel) inside the reference ellipsoid, representing the stochastic current density $\mathbf{J}(\mathbf{r})$ inside ΔV, the incident electric field from the plume formation to radiometer antenna is computed from the radiation integral at the far field.

Assuming fluctuating current sources $\mathbf{J}(\mathbf{r})$ inside the ellipsoid formation, the electric field produced on the aperture of a distant antenna as shown in Fig. 3 is computed by the equation [6]:

$$\dot{E} = -j\omega\mu_o \frac{e^{-jk_oR}}{4\pi R} e^{-a_oR} \iiint_{\substack{\text{Ellipsoid}\\ \text{Volume}}} \mathbf{J}(\mathbf{r}) e^{-k_i l(x,y,z)} e^{jk_r l(x,y,z)} d\mathbf{r} \tag{9}$$

where $\mu_o = 4\pi \times 10^{-7}$ (H/m) is the free space magnetic permeability.

R the average antenna — ellipsoid distance

$\frac{e^{-jk_oR}}{4\pi R}$ the free space spherical wave factor

e^{-a_oR} the attenuation factor in the air

$e^{-k_i l(x,y,z)} e^{jk_r l(x,y,z)}$ the propagation inside the ellipsoid starting at point (x, y, z) and ending on the line emerging of the ellipsoid and connecting the antenna.

Since $\mathbf{J}(\mathbf{r})$ is a stochastic vector, and $\dot{\mathbf{E}}$ is also stochastic, it is necessary to compute the ensemble average $\langle \mathbf{E} \cdot \mathbf{E}^* \rangle$ related to antenna signal output ($\mathbf{E}^*$ = complex conjugate of $\mathbf{E}$).

While since $\langle \mathbf{J}(\mathbf{r}) \rangle = 0$, $\langle \dot{\mathbf{E}} \rangle = 0$.

Following the fluctuation-dissipation theorem [7]

$$\left\langle \mathbf{J}(\mathbf{r}) \cdot \mathbf{J}^* \left(\mathbf{r}'\right) \right\rangle = \frac{4k_B T\sigma}{\pi} \delta\left(\mathbf{r} - \mathbf{r}'\right) \tag{10}$$

where $k_B = 1,38 \times 10^{-23}$ (J/K) Boltzmann constant, $T =$ Temperature, $\sigma =$ conductivity, $\delta(\mathbf{r}) =$ three-dimensional delta function.

Eq. (10) is valid at frequencies $\hbar\omega \ll kT$, with $\hbar = h/(2\pi)$, $h = 6,28 \times 10^{-34}$ Js.

In general case: $kT \to \frac{\hbar\omega}{2} \coth \frac{\hbar\omega}{2k_BT}$ if the photon energy $\hbar\omega > kT$.

Utilizing Eq. (9) with (10), the ensemble average $\langle \mathbf{E} \cdot \mathbf{E}^* \rangle$ is found to be:

$$\left\langle \dot{\mathbf{E}} \cdot \dot{\mathbf{E}}^* \right\rangle = (\omega\mu_o)^2 \frac{e^{-2a_oR}}{(4\pi R)^2} \iiint_{\substack{\text{Ellipsoid}\\ \text{Volume}}} e^{-2k_i l(x,y,z)} \frac{4kT\sigma}{\pi} d\mathbf{r} \tag{11}$$

The quantity $E^2 = \langle \dot{\mathbf{E}} \cdot \dot{\mathbf{E}}^* \rangle$ is related to incident power density (W/m^2) to antenna which is equal to

$$P_{\text{inc}} = \frac{E^2}{2Z_o}, \quad Z_o = 120\pi\ (\Omega) \tag{12}$$

being the free space wave impedance.

The radiometric signal power at the antenna output can be computed by taking into account the effective electromagnetic area $A_e = \left(\frac{\lambda^2}{4\pi} G_o\right)$ of the antenna, which is obtained from the antenna gain G_o with the following relations:

$$\frac{\langle VV^* \rangle}{2Z_{oo}} = \frac{E^2}{2Z_o} \left(\frac{\lambda^2}{4\pi} G_o\right) \tag{13}$$

$\langle VV^* \rangle$ the antenna output power

$Z_{oo} =$ the antenna output transmission line impedance $= 50\,\Omega$

$\lambda =$ the radiated wavelength

Using Eqs. (12), (13), $\lambda = 2\pi c/\omega$ and substituting into Eq. (11) into (13):

$$\frac{\langle VV^* \rangle}{2Z_{oo}} = \frac{(c\mu_o)^2}{2Z_o} \frac{BG_o e^{-2a_o R}}{(4\pi R)^2} I(a,b,k_i,\hat{s})\, 4k \tag{14}$$

in which the term $I(a,b,k_i,\hat{s})$, in case the plume consists of single ellipsoid, can be written as follows:

$$I(a,b,k_i,\hat{s}) = \iiint_{\substack{\text{Spheroid}\\ \text{Volume}}} T(r)\,\sigma(r)\, e^{-2k_i l(x,y,z)} d\mathbf{r} \tag{15}$$

a, b refer to ellipsoid minor and major axis lengths (see Fig. 3).

$\hat{s} = s_x\hat{x} + s_y\hat{y} + s_z\hat{z}$ is the unit vector along the propagation vector connecting the point (x,y,z) with receiving antenna.

Write explicitly in Eq. (15):

$$I(a,b,k_i,\hat{s}) = \int_{-b}^{b} dz' \int_{-\sqrt{a^2-\frac{z'^2a^2}{b^2}}}^{\sqrt{a^2-\frac{z'^2a^2}{b^2}}} dx' \int_{-\sqrt{a^2-\frac{z'^2a^2}{b^2}-x'^2}}^{\sqrt{a^2-\frac{z'^2a^2}{b^2}-x'^2}} dy' e^{-2k_i l} T(r)\sigma(r) \tag{16}$$

where l represents the path length of wave originating from an internal point (x',y',z'), travelling along the unit $\hat{s}$, and emerging from the ellipsoid surface:

$$l = \left[\sqrt{\left(\frac{x's_x+y's_y}{a^2}+\frac{z's_z}{b^2}\right)^2 - \left(\frac{s_x^2+s_y^2}{a^2}+\frac{s_z^2}{b^2}\right)\left(\frac{x'^2+y'^2}{a^2}+\frac{z'^2}{b^2}-1\right)} - \left(\frac{x's_x+y's_y}{a^2}+\frac{z's_z}{b^2}\right)\right]\left(\frac{1}{\frac{s_x^2+s_y^2}{a^2}+\frac{s_z^2}{b^2}}\right)$$

In the following, the value of Eq. (16) $I(a,b,k_i,\hat{s})$ integral is computed numerically.

In the case of plume consisting of multiple ellipsoids, as shown in Fig. 2, the integral term of Eq. (15) is generalized by adding and subtracting the contributions of each volume with different conductivities $\sigma_i(r)$ and temperatures $T_i(r)$ with $i = 1,2,3,...$, and the power output at the receiving antenna is computed by the superposition principle:

$$\frac{\langle VV^* \rangle}{2Z_{oo}} = \frac{(c\mu_o)^2}{2Z_o} \frac{BG_o e^{-2a_o R}}{(4\pi R)^2} I_\Sigma 4k_B \tag{17}$$

where

$$I_\Sigma = \left[T_1\sigma_1 I(a_1,b_1,k_{i1},\hat{s}) + T_2\sigma_2\left(I(a_2,b_2,k_{i2},\hat{s}) - I(a_1,b_1,k_{i2},\hat{s})\right) + T_3\sigma_3\left(I(a_3,b_3,k_{i3},\hat{s}) - I(a_2,b_2,k_{i3},\hat{s})\right) + ...\right] \tag{18}$$

If $T_1\sigma_1 = T_2\sigma_2 = T_3\sigma_3...$ in Eq. (18), the term inside the bracket is simplified to $T_3\sigma_3 I(a_3,b_3,ki_3,\hat{s})$.

2.3. Computation of Detection Range

In order to compute the detection range R of an aircraft by a radiometer receiver, one has to compare the power received by an antenna of the emitted radiation by the exhaust plume with the radiometer temperature measurement resolution.

By writing Eq. (17) after placing $c\mu_0 = 120\pi = Z_0\,(\Omega)$ and defining the equivalent "target" temperature T_{radi}:

$$\frac{\langle VV^* \rangle_{\text{radi}}}{2Z_{oo}} = k_B T_{\text{radi}} \tag{19}$$

it is found that:

$$T_{\text{radi}} = \frac{15BG_o e^{-2a_o R} I_\Sigma}{\pi R^2} = 4,77\,\frac{BG_o e^{-2a_o R} I_\Sigma}{R^2} \tag{20}$$

Then, T_{ther} is defined as the total "noise" power when radiometer is "looking" to a load with an equal temperature. Considering the availability today of cryogenic low noise amplifiers, we take $T_{\text{ther}} = 4°\text{K}$. The antenna observing signals towards sky observes an apparent temperature T_A which at high elevation angle is approximately $T_A = 4°\text{K}$.

To compute the temperature resolution of the radiometer the well-known equation is used [8]:

$$\delta\text{T} = \frac{T_{\text{ther}} + T_A}{\sqrt{B\tau}} \tag{21}$$

where $B =$ the radiometer input bandwidth (Hz) and $\tau =$ the post detection integration time (sec).

If $B = 100\,\text{MHz}$ and $\tau = 1\,\mu\text{s}$, then

$$\delta\text{T} = \frac{8}{10} = 0,8°\text{K}$$

The same low δT could be achieved by decreasing the bandwidth B and increasing the post detection integration time τ (i.e., $B = 10\,\text{MHz}$, $\tau = 10\,\mu\text{s}$).

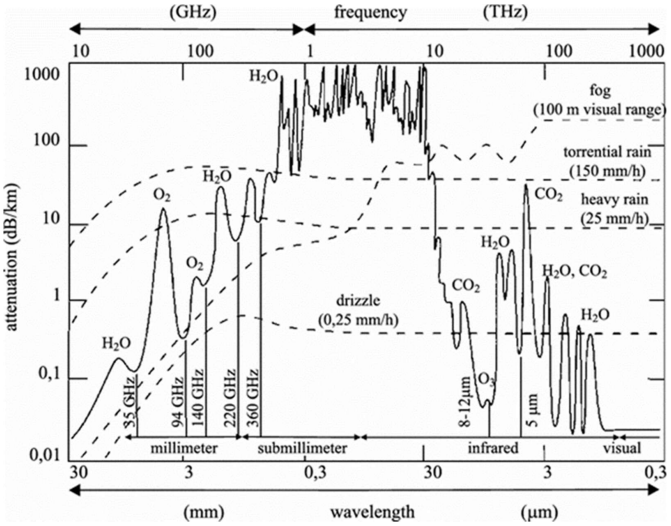

FIGURE 4. Atmospheric attenuation (in dB/Km) for different wavelengths [11].

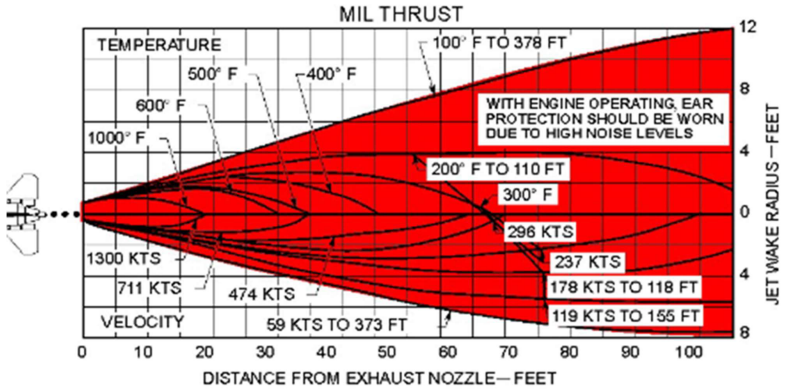

FIGURE 5. Reference exhaust gas plume formation [12].

Then, we define the range at which $T_{radi} = \delta T = 0,8°K$, and therefore from Eq. (21):

$$R_{\text{detection}} e^{a_0 R_{\text{detection}}} = \sqrt{11,95 \cdot B \cdot G_0 I_\Sigma} \tag{22}$$

If α_0 is small at low microwave frequencies, the equation is simplified.

2.4. Attenuation of Electromagnetic Radiation in Plasma and Atmosphere

The gases in air which primarily attenuate electromagnetic radiation are O_2 and water vapor (H_2O). The strength of the absorption depends largely on the wavelength of the radiation.

In contrast to IR options, the use of the radio frequency band (radiometry) offers the possibility of reduced propagation losses of electromagnetic radiation, as shown in Fig. 4. It is obvious that the effect of vapor and oxygen on the mm scale is reduced. In the radio wave band (mm), O_2 creates a large attenuation between 50 GHz and 70 GHz, with higher absorption at two frequencies, 60 GHz and 118,75 GHz, respectively [9, 10]. However, there are wide spectrum widths with reduced attenuation. In particular, in the discrete low attenuation and wide propagation windows of 35, 94, 140, 220, 360 GHz, the attenuation is characteristically low [11].

3. NUMERICAL COMPUTATIONS

In order to examine the achievable detection ranges of the proposed method, a reference plume formation is taken as shown in Fig. 5 for an aircraft flying at cruise speed ($\sim$ 80% of thrust) [12].

Converting the temperatures in plume of Fig. 5 from Fahrenheit to Kelvin and combining the respective dimensions of the ellipsoids yields Table 1.

To calculate the detection range R of the radiometry system to detect the aircraft of the specific case, it is necessary to calculate the following parameters:

Plasma electron number N_e (per ellipsoid): takes values per ellipsoid, respectively, from the 1st to the 6th: 5×10^9, 1×10^9, 5×10^8, 1×10^8, 5×10^7, 1×10^7 (data from working measurements), as shown in Fig. 6.

TABLE 1. Characteristics of the ellipsoid model of the exhaust plume.

Ellipsoid	Minor axis (m)	Major axis (m)	Temperature (°K)
1	0,34	5,18	678
2	0,54	9,14	489
3	0,68	11,58	444
4	0,8	19,82	400
5	1,22	27,44	355
6	3,36	85,34	311

Frequency f_p:

$$\mathbf{f}: 0.3, 1, 10.5, 22, 35, 51.5, 72.5, 94, 140, 220, 360, 1000, 3000\,\text{GHz and } f = \frac{\omega_p}{2\pi} \tag{23}$$

for ω (angular frequency): 1.88, 6.28, 65.94, 138.16, 219.8, 323.42, 455.3, 590.32, 879.2, 1381.6, 2260.8, 6280, 18840 rad/sec.

Plasma frequency, given by:

$$\omega_p = \sqrt{\frac{N_e e^2}{m_e \varepsilon_o}} \tag{24}$$

where numerically $\omega_p = 5,64 \times 10^4 \times N_e^{1/2}$ (rad/sec).

Plasma electron collision frequency, given by:

$$\nu_e = 2,91 \cdot 10^{-5} \cdot N_e \cdot \left(\frac{T}{11600}\right)^{-3/2} \tag{25}$$

The collision frequencies of neutral electrons, based on laboratory results, are shown in Fig. 7.

The conductivity of an aircraft exhaust gas is

$$\sigma = \left(\frac{\omega_p}{\omega}\right)^2 \cdot \nu_e \cdot \varepsilon_o \tag{26}$$

and from this the attenuation inside the exhaust plasma volume is:

$$\alpha = \left(\frac{1}{2c}\right) \cdot \left(\frac{\omega_p^2 \cdot \nu_e}{\omega^2 + \nu_e^2 - \omega_p^2}\right) \tag{27}$$

Based on the data of Fig. 5 and Table 1, we calculate and present, in the following Tables 2 and 3, the pertinent parameters in the previous analysis [Eqs. (18)–(27)]. Calculations were made of the range of electromagnetic radiation received from an antenna separately per ellipsoid and for all ellipsoids for different frequencies. Indicatively, the following tables show plume characteristics and detection range values R for all the aforementioned frequencies for respective G_o.

In order to carry out a feasibility study on the use of radiometric detection of jet engine exhaust gas plumes, we assume a receive antenna with an effective area A_e described by a circle of radius $\alpha = 25$ cm and $A_e = \pi\alpha^2$. Then, for each frequency, the antenna gain is computed with the equation $G_O = 4\pi A_e/\lambda^2$, $\lambda = c/f$ and $G_O\,(\mathrm{dB}) = 10\log_{10}(G_O)$. In Table 3, detection ranges for 13 cases are given. As shown at 22 and 35 GHz frequencies, detection ranges of 60 km can be achieved.

Based on the data of Table 3, the ranges of electromagnetic radiation received from an antenna for all ellipsoids for different frequencies are presented in Fig. 8.

TABLE 2. Plume characteristics for various frequencies for each individual ellipsoid.

Ellipsoid	Minor semi-axis (a_i) (m)	Major semi-axis (b_i) (m)	Electron Temperature T_i (^{o}K)	Electron density n_{ei} (cm^{-3})	Electron Collision frequency ν_{ei} (sec^{-1} x 10^8)	Plasma frequency ω_p (rad/sec x 10^9)	angular freuency ω (rad/sec x 10^9)	Radiometry radio frequency f (GHz)	Permittivity of free space ε_o (C^2/N.m^2)	Conductivity σ_i	Attenuation α_i
1	0,17	2,59	678	5E+09	0,10297	3,988	1,88	0,3	8,854E-12	4,0852E-04	-2,2092E-02
							6,28	1		3,6767E-05	1,1598E-02
							65,94	10,5		3,3348E-07	6,3005E-05
							138,16	22		7,5964E-08	1,4311E-05
							219,8	35		3,0014E-08	5,6516E-06
							323,42	51,5		1,3862E-08	2,6098E-06
							455,3	72,5		6,9948E-09	1,3168E-06
							590,32	94		4,1610E-09	7,8330E-07
							879,2	140		1,8758E-09	3,5311E-07
							1381,6	220		7,5964E-10	1,4300E-07
							2260,8	360		2,8369E-10	5,3402E-08
							6280	1000		3,6767E-11	6,9209E-09
							18840	3000		4,0852E-12	7,6899E-10
2	0,27	4,57	489	1E+09	0,03362	1,784	1,88	0,3	8,854E-12	2,6678E-05	4,8370E-02
							6,28	1		2,4010E-06	4,9162E-04
							65,94	10,5		2,1778E-08	4,1025E-06
							138,16	22		4,9608E-09	9,3397E-07
							219,8	35		1,9600E-09	3,6897E-07
							323,42	51,5		9,0528E-10	1,7041E-07
							455,3	72,5		4,5679E-10	8,5987E-08
							590,32	94		2,7173E-10	5,1151E-08
							879,2	140		1,2250E-10	2,3060E-08
							1381,6	220		4,9608E-11	9,3381E-09
							2260,8	360		1,8526E-11	3,4874E-09
							6280	1000		2,4010E-12	4,5196E-10
							18840	3000		2,6678E-13	5,0218E-11
3	0,34	5,79	444	5E+08	0,01943	1,261	1,88	0,3	8,854E-12	7,7087E-06	2,6292E-03
							6,28	1		6,9378E-07	1,3609E-04
							65,94	10,5		6,2928E-09	1,1850E-06
							138,16	22		1,4334E-09	2,6985E-07
							219,8	35		5,6635E-10	1,0661E-07
							323,42	51,5		2,6158E-10	4,9241E-08
							455,3	72,5		1,3199E-10	2,4846E-08
							590,32	94		7,8518E-11	1,4780E-08
							879,2	140		3,5397E-11	6,6631E-09
							1381,6	220		1,4334E-11	2,6983E-09
							2260,8	360		5,3533E-12	1,0077E-09
							6280	1000		6,9378E-13	1,3060E-10
							18840	3000		7,7087E-14	1,4511E-11

4	0,4	9,91	400	1E+08	0,00454	0,564	1,88	0,3	8,854E-12	3,6060E-07	7,4561E-05
							6,28	1		3,2454E-08	6,1588E-06
							65,94	10,5		2,9437E-10	5,5415E-08
							138,16	22		6,7054E-11	1,2622E-08
							219,8	35		2,6493E-11	4,9871E-09
							323,42	51,5		1,2236E-11	2,3034E-09
							455,3	72,5		6,1744E-12	1,1623E-09
							590,32	94		3,6729E-12	6,9139E-10
							879,2	140		1,6558E-12	3,1169E-10
							1381,6	220		6,7054E-13	1,2622E-10
							2260,8	360		2,5042E-13	4,7138E-11
							6280	1000		3,2454E-14	6,1091E-12
							18840	3000		3,6060E-15	6,7879E-13
5	0,61	13,7	355	5E+07	0,00272	0,399	1,88	0,3	8,854E-12	1,0782E-07	2,1249E-05
							6,28	1		9,7041E-09	1,8341E-06
							65,94	10,5		8,8019E-11	1,6569E-08
							138,16	22		2,0050E-11	3,7742E-09
							219,8	35		7,9217E-12	1,4912E-09
							323,42	51,5		3,6588E-12	6,8873E-10
							455,3	72,5		1,8462E-12	3,4753E-10
							590,32	94		1,0982E-12	2,0673E-10
							879,2	140		4,9511E-13	9,3199E-11
							1381,6	220		2,0050E-13	3,7742E-11
							2260,8	360		7,4877E-14	1,4095E-11
							6280	1000		9,7041E-15	1,8267E-12
							18840	3000		1,0782E-15	2,0297E-13
6	1,68	42,7	311	1E+07	0,00066	0,178	1,88	0,3	8,854E-12	5,2599E-09	9,9907E-07
							6,28	1		4,7339E-10	8,9182E-08
							65,94	10,5		4,2938E-12	8,0826E-10
							138,16	22		9,7808E-13	1,8411E-10
							219,8	35		3,8644E-13	7,2743E-11
							323,42	51,5		1,7849E-13	3,3598E-11
							455,3	72,5		9,0062E-14	1,6953E-11
							590,32	94		5,3575E-14	1,0085E-11
							879,2	140		2,4152E-14	4,5464E-12
							1381,6	220		9,7808E-15	1,8411E-12
							2260,8	360		3,6527E-15	6,8758E-13
							6280	1000		4,7339E-16	8,9110E-14
							18840	3000		5,2599E-17	9,9011E-15

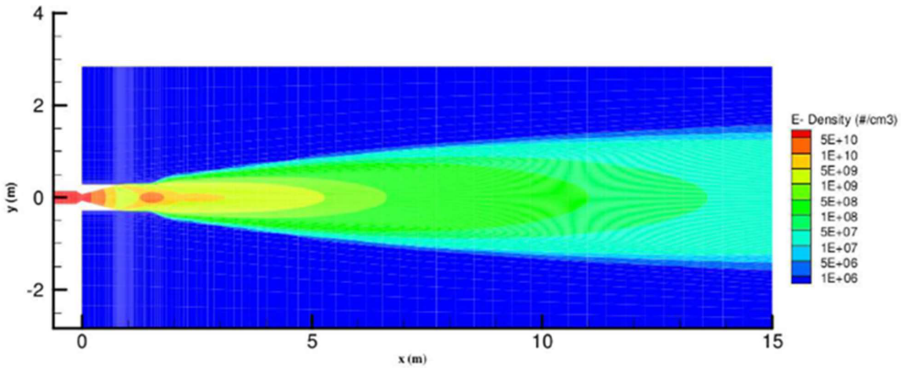

FIGURE 6. Electron number density [13].

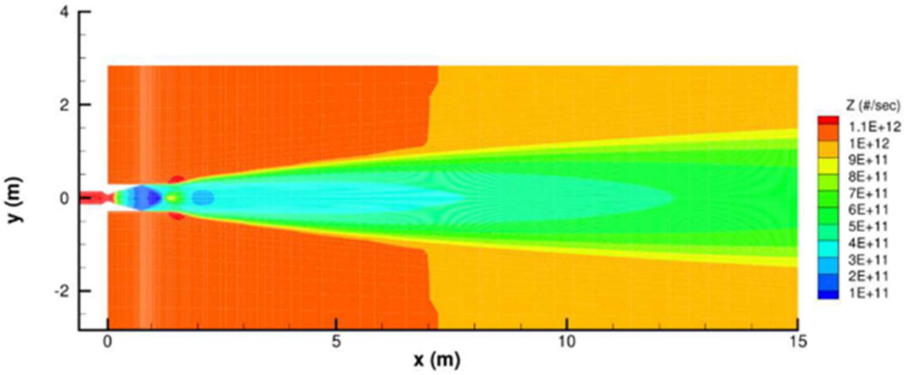

FIGURE 7. Neutral electron collision frequency contours [14].

TABLE 3. Detection range values R for various frequencies from plasma ellipsoids.

Cases	Radiometry radio frequency f (GHz)	Antenna Gain G_o (dB)	Atmospheric attenuation α_o (Neper/km)	**Detection Range R (km)**
1	0,3	3,92	0,0000011	**71,83**
2	1	14,38	0,0005300	**68,85**
3	10,5	34,80	0,0013246	**65,19**
4	22	41,22	0,0025152	**61,33**
5	35	45,26	0,0031761	**59,28**
6	51,5	48,61	0,1996288	**9,91**
7	72,5	51,58	0,1006095	**15,32**
8	94	53,84	0,0131673	**41,46**
9	140	57,30	0,0516380	**22,45**
10	220	61,22	0,2017478	**9,84**
11	360	65,50	0,2369234	**8,83**
12	1000	74,38	1,0000000	**3,13**
13	3000	83,92	1,0000000	**3,13**

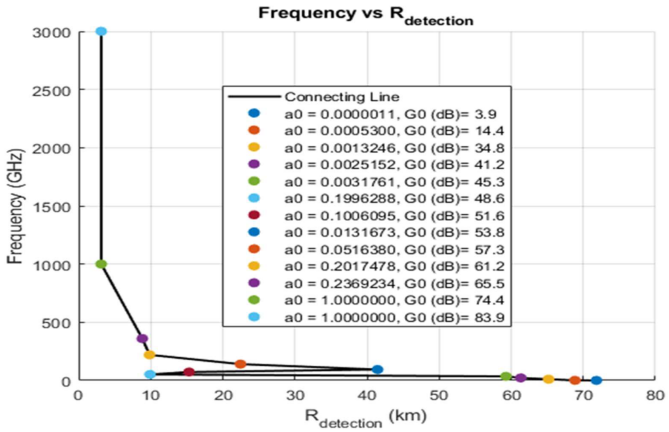

FIGURE 8. Detection range values R for various frequencies from all plasma ellipsoids.

4. CONCLUSIONS

A feasibility study has been conducted to examine the possibility of using passive radiometry methods to detect aircrafts with jet engine propulsion. Electromagnetic analysis method is adopted to compute the received chaotic radiation from the exhaust gas plumes by a directive passive radiometer receiver. The detection range is computed by comparing the received power with radiometer resolution. A general electromagnetic formulation and data obtained from exhaust gas properties published previously of the low-density plasma are used to compute the detection range for the UHF to Terahertz waves. Specifically, frequencies used for radioastronomy observations were selected since these frequencies are expected to be free of man-made transmissions. Atmospheric attenuation was also included in the model. The early results presented shows that detection ranges at 10–100 GHz frequencies could be as high as 50 km. These results should be considered as preliminary. Issues such as angular scanning of the space, triangulations between several radiometer positions, detection and false alarm need to be addressed based on the presented analysis.

REFERENCES

[1] Winther, M. and K. Rypdal, 1.A.3.a, 1.A.5.b Aviation, European Environment Agency, 2017.

[2] Starik, A. M., "Gaseous and particulate emissions with jet engine exhaust and atmospheric pollution," *Advance on Propulsion Technology for High-Speed Aircraft*, Vol. 15, 1–22, 2008.

[3] He, L., Y. Zhang, H. Zeng, and B. Zhao, "Research progress of microwave plasma ignition and assisted combustion," *Chinese Journal of Aeronautics*, Vol. 36, No. 12, 53–76, 2023.

[4] Haverkamp, H., S. Wilhelm, A. Sorokin, and F. Arnold, "Positive and negative ion measurements in jet aircraft engine exhaust: Concentrations, sizes and implications for aerosol formation," *Atmospheric Environment*, Vol. 38, No. 18, 2879–2884, 2004.

[5] Stix, T. H., *Waves in Plasmas*, Chapter 1, Springer Science & Business Media, New York, 1992.

[6] Jones, D. S., *Theory of Electromagnetism*, Chapter 2, Pergamon Press, 1962.

[7] Tsang, L., J. A. Kong, and R. T. Shin, *Theory of Microwave Remote Sensing*, 42, John Wiley, New York, 1985.

[8] Racette, P. and R. H. Lang, "Radiometer design analysis based upon measurement uncertainty," *Radio Science*, Vol. 40, No. 05, 1–22, 2005.

[9] Singh, H., V. Kumar, B. Bonev, and K. Saxena, "A novel method for prediction of attenuation of millimeter waves by fog and smoke," *International Journal of Recent Technology and Engineering (IJRTE)*, Vol. 8, No. 3, 2080–2085, Sep. 2019.

[10] Frey, T. L., "The effects of the atmosphere and weather on the performance of a mm-Wave communication link," *Applied Microwave and Wireless*, Vol. 11, 76–81, 1999.

[11] Preissner, J., "The influence of the atmosphere on passive radiometric measurements," *AGARD Millimeter and Submillimeter Wave Propagation and Circuits*, 1979.

[12] Technical order 00-105E-9, Revision 11, Chapter 8, Aerospace Emergency Rescue and Mishap Response Information, F-16 aircraft danger areas, Engine Thrusts for F100-PW-229, Feb. 2006.

[13] Coutu, N., W. Barrot, W. Engblom, and E. Perrell, "Implementation of microwave transmissions for rocket plume diagnostics," in *2013 Proceedings of IEEE Southeastcon*, Jacksonville, FL, USA, 2013.

[14] Delaney, B. T., B. A. Zetlen, R. C. Tai, G. D. Seitchek, and G. G. Elcock, "Aircraft engine exhaust plume dynamics," Science and Engineering Associates Inc., Seattle, WA, USA, 1986.